Scale-up in laminar and transient regimes of a multi-stage stirrer, a CFD approach

B. Letellier[a], C. Xuereb[b,*], P. Swaels[a], P. Hobbes[a], J. Bertrand[b]

[a] *Cray Valley (ATOFINA), Centre de Recherche de l'Oise Parc Alata, BP 22-60550 Verneuil en Halatte, France*
[b] *Laboratoire de Génie Chimique, CNRS UMR 5503, 18, Chemin de la Loge, 31078 Toulouse Cedex 4, France*

Abstract

A multi-stage industrial agitator system adapted to the mixing of a mixture whose viscosity varies during the process has been characterized by using CFD. In the entire study the mixture is supposed to have a Newtonian behavior even though it is rarely the case. It is shown that the well-adapted propeller is able to efficiently blend high viscous media provided the Reynolds number is not too low. A scale-up study of the agitated system has also been carried out by respecting the classical scale-up rules such as the geometrical similarity and the conservation of the power per volume in the particular case of viscous media.

Using an Eulerian approach, the hydrodynamics of three different scales with geometrical similarity have been numerically characterized by the energy curve (power number versus Reynolds number) and by the Metzner and Otto constant in which both are required for scale-up procedure. Experimental power measurements have been carried out at the smaller scale so that simulations have been partially validated. New hydrodynamic criteria have also been introduced in order to quantify the flows in the case of a multi-stage stirrer running at low Reynolds number. It has been shown how this hydrodynamic differs dramatically from one scale to another when scale-up at constant energy per volume is applied. From the CFD results, recommendations about the widely used scale-up rules have been suggested and modifications of stirring geometry have been proposed in order to reduce the flow pattern variations during scale-up.

Keywords: Laminar mixing; Scale-up; CFD; Double-flux impeller; Multi-stage stirrer

1. Introduction

Industrial mixing in the laminar regime is usually performed by means of specific stirrers like anchors (Takahashi, Arai, & Saito, 1980), screws (Aubin, Naude, Xuereb, & Bertrand, 2000) or helical ribbons (Brito-de la Fuenta, Choplin, & Tanguy, 1997). These stirrers are well designed for processes involving highly viscous mixtures (> 50 Pa s) of Newtonian or non-Newtonian fluid but, if the mixture viscosity decreases, their efficiency decreases. In industrial processes (e.g. polymerization, fermentation or several other processes), the viscosity changes of the mixture occur frequently and, therefore, there are needs to modify the mixing conditions (Gerstenberg, Sckuhr, & Steiner, 1983). A solution could consist in combining different kinds of stirrers, for example, an helical ribbon with a Rushton turbine (Tanguy, Thibault, La Fuente, Espinoza-Solares, & Jecante, 1997), which has however the drawback of requiring two different motors in the mixing unit. A second alternative is to improve the performance in laminar conditions of a common stirring system such as propellers. According to Dickey (2000), this can be achieved using several stages of propellers whose diameters have been increased ($D/T > 0.9$) and by removing baffles. Such stirring systems are then able to blend highly viscous mixtures until about 30 Pa s and remain also efficient for Reynolds number varying from 20 to the turbulent regime. The purpose of this CFD work is, on one hand, to investigate such a stirring system and, on the other hand, to study the scale-up of this industrial process.

Many rules or principles can be applied for the scale-up of stirring vessels. According to Uhl and Von Essen (1986), the following types of similarity have to be used: geometric, kinematics and dynamic. Kinematics similarity means that the fluid motion is similar provided the geometrical

similarity is respected. The dynamic similarity is based on the conservation of the forces ratio such as the Reynolds number, Froude number, Weber number, etc. It is however clear that no more than two ratios can be kept constant and all other criteria are consequently violated. Therefore, it is important during scale-up to recognize those main criteria which, for further success, must be satisfied at each scale. In some particular cases, other principles like thermal and chemical similarity also have to be considered. For example, it could be essential to keep the heat transfer per unit of mass or a thermal coefficient constant in the case of polymer reactors. Nevertheless, it has to be pointed out here that thermal similarity can lead to inconvenient processes. In addition, the chemical similarity can be justified if certain kinetics have to be maintained. The most widely used scale-up rule is the equal power per unit of volume (Büche recommendations). As noted by Gerstenberg et al. (1983), the power per volume criteria is often applied in practice and, in many instances, has given accurate results. Therefore, it can be retained as a basic scale-up criterion and this is the reason why it has been chosen for this study.

The main purpose of this work is to evaluate the consequences of such scale-up criteria on the hydrodynamics of the agitated vessel. This study attempts to demonstrate why geometrical similarity must not be applied blindly without taking care of any change of the hydrodynamic regime. Thanks to CFD, it has been shown how, with geometrical similarity, the flow patterns vary as a function of the scale during scale-up with a constant power per volume. This useful visualization can be used to modify the stirring system at the smallest scale in order to ensure the same hydrodynamics during scale-up of processes where hydrodynamics are critical.

The scale-up rules of equal power per volume differ with the hydrodynamic regime characterizing the process. In turbulent flow ($Re > 10,000$), the power number given by Eq. (1) remains constant and the power per volume unit varies as shown in Eq. (2).

$$P_o = \frac{P}{\rho N^3 D^5}, \tag{1}$$

$$P/V = P_o \beta \frac{4\rho}{\pi} \left(\frac{D}{H}\right) \left(\frac{D}{T}\right)^2 N^3 D^2, \tag{2}$$

where β is a factor depending on the bottom geometry of the vessel ($\beta = 1$ in the case of a flat bottom vessel). Assuming constant geometry, the equal per volume criterion then leads to the following scale-up rule given by

$$N^3 D^2 = \text{constant (or } ND^{2/3} = \text{constant}). \tag{3}$$

However, in the case of a laminar flow ($Re < 20$), the power number is inversely proportional to the Reynolds number as in the following:

$$P_o\, Re = A. \tag{4}$$

The laminar energy constant, A, theoretically depends on the agitator type and on the system geometry only. The power per unit of volume is varying in laminar regime as shown below:

$$P/V = A \frac{4\mu}{\pi} \beta \left(\frac{D}{H}\right) \left(\frac{D}{T}\right)^2 N^2. \tag{5}$$

Then, by keeping the power per volume unit constant in the case of geometrical similarity and for the same mixture, Eq. (5) leads to the scale-up rule specified by

$$N = \text{constant (or } ND^0 = \text{constant}). \tag{6}$$

During scale-up, the Reynolds number increases as the impeller diameter increases and, therefore, a laminar regime at small scale may become a transient or even turbulent regime at higher scales. In the transient regime, the two scale-up rules given by both Eqs. (3) and (6) become unsuitable and cannot be applied. The energy curve in the transient regime is then needed to scale-up by constant power per volume criterion.

This paper presents a scientific approach of the scale-up at constant power per unit of volume in the case of a process in the laminar or transient regime. Using CFD, the energy curve for the three scales of similar geometry in laminar and transient regime were drawn. Power measurements were carried out so that the CFD results could be partially validated. As explained by Aubin et al. (2000), there are not a lot of experimental techniques available for the local hydrodynamic characterization of high viscosity fluids. The classic techniques, such as laser Doppler velocimetry (LDV) and particle image velocimetry (PIV), which allow local measurements using a penetrating laser beam are limited in such high viscosity fluids due to light diffusion. From the energy curve, stirring speed can be set at each scale to ensure a scale-up by constant power per volume criterion. With these stirring conditions, a local analysis of the flow patterns is carried out in order to characterize the hydrodynamic performance induced by the use of such scale-up criteria.

2. System description and method

2.1. Description of the stirring system

The stirring system studied in this paper is used in industrial processes. Considering the high viscosity of the Newtonian fluid to be mixed at the beginning of the process, baffles become useless and have therefore been removed. According to the recommendations given by Dickey (2000) for high viscosity mixing with common propellers, several impellers with larger diameter should be chosen. In addition to the justifications put forward by Dickey (2000), the large impeller diameter and the absence of baffles leads to improvements in thermal performances which are essential in industrial processes. Although the viscosity at the end of the process becomes very low (0.05 Pa s), the stirring system involving axial impellers provides suitable mixing. It has

	Scale		
	a	b	c
Double-Flux Propellers diameter, D (m)	0.36	1.80	2.61
Pitched Blade Turbine diameter, D' (m)	0.24	1.20	1.74
Vessel Diameter, T (m)	0.40	2.00	2.90
Vessel Height, H (m)	0.27	1.37	1.96
Distance Bottom – PBT, H_1 (m)	0.04	0.20	0.29
Distance PBT-DF, H_2 (m)	0.12	0.60	0.87
Vessel Volume (m^3)	0.03	3.8	11.5
Linear scale-up factor, α	1	5	7.25

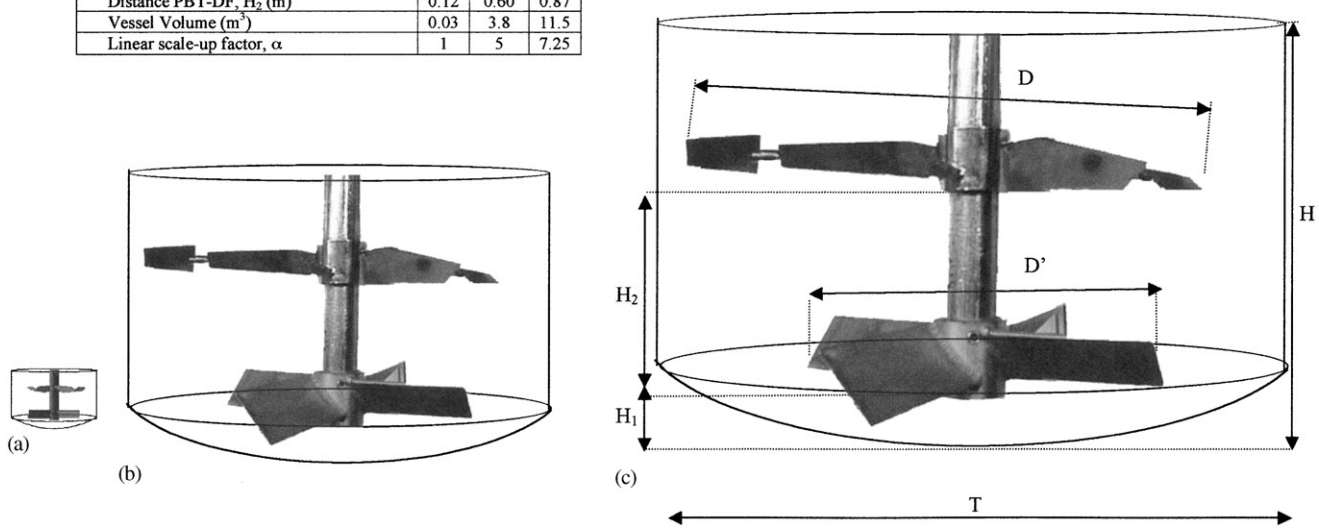

Fig. 1. Scale-up of a multi-stages stirrer, geometrical parameters at scales studied.

however to be underlined that the aim of the study is not to model the process during the variation of mixture viscosity.

As shown in Fig. 1, the stirring system involves a MIG double-flux (DF) impeller ($D/T = 0.9$) and a four-bladed pitched blade turbine (PBT) ($D/T = 0.6$), which is located at the bottom of the vessel. Performances of MIG DF impellers have been compared to those of helical ribbon by Käppel (1979). He recommended a DF diameter ratio of 0.9 to attain the best efficiency for mixing highly viscous liquids. At least, it can be noted in Fig. 1 that a dished bottom is used as it is common in industrial processes.

As announced by suppliers of the DF stirrers, these kind of DF impellers provide excellent blending of highly viscous media and diameter ratios up to 0.95 can be used to mix products with viscosities of up to 80 Pa s. The opposed blade angles at the tip of the DF impeller provide an upward flow and good mixing close to the wall. In addition to its relatively low-energy consumption, the main advantage of the DF impeller is that the flows induced by the inner and outer sections move in opposite directions, improving the distribution of the mechanical energy in the vessel.

Three stirring vessels **a**, **b** and **c** are to scale with one another and each has been meshed with the geometrical dimensions as summarized in Fig. 1.

2.2. CFD method

Simulations of three-dimensional velocity fields and energy consumption have been performed with the commercial code Fluent® 5, functioning with unstructured mesh, which enables the representation of the real stirring geometry. The CFD code has been used to solve, in Cartesian co-ordinates, the continuity and momentum equations for a laminar flow. Several agitator speeds have been simulated with Newtonian and non-Newtonian fluids. Their characteristics and rheological behavior are summarized in Table 1.

Resolution of the algebraic equations was performed using the semi-implicit algorithm pressure linked equation (SIMPLE) with a second-order upwind discretization scheme. Constant boundary conditions have been set respecting an rotating reference frame (RRF) approach. Here, the impeller is kept stationary and the flow is steady relative to the rotating frame, while the outer wall of the vessel is given an angular velocity equal and opposite to the velocity of the rotating frame. This approach can be employed due to the absence of baffles (and thus baffle–impeller interaction) in the real industrial configuration. The same RRF approach, often used for stirred vessels, has given accurate results for several different stirring systems in laminar (Aubin et al., 2000) and turbulent flow (Naude, 1998). The simplification of the stirring system where baffles have been removed is obviously independent of the CFD resolution and is only due to mixing and industrial considerations. In the case of agitated vessels involving baffles, computational flow could nonetheless have been easily achieved with an MRF (Naude, 1998) or sliding meshes approaches. Since no vortex appears, the free surface is defined as a symmetrical boundary condition where the normal velocity component is equal to zero. Solutions are considered to be converged when repeated iterations do not change the power consumption and when the dimensionless velocity residuals remain

Table 1
Fluids characteristics used for simulations and experimental measurements

	Rheological nature	Viscosity, μ (Pa s)	Consistency index, m ($kg\,s^{n-2}\,m^{-1}$)	Flow behaviour index, n	Specific gravity, ρ ($kg\,m^{-3}$)
Simulations scales **a**, **b** and **c**	Newtonian	30	—	—	1000
	Newtonian	5	—	—	1000
	Shear thinning (power law)	—	70	0.3	1000
	Shear thinning (power law)	—	70	0.7	1000
Experiments scale **a**	Newtonian 25°C	4.2	—	—	1100

Table 2
Mesh optimization for a Newtonian fluid: viscosity of 30 Pa s and specific gravity of 1000 $kg\,m^{-3}$

	Scales					
	a		**b**		**c**	
Stirring speed N (rpm)	90		70		50	
Number of cells (half volume)	35 644	75 951	58 053	104 153	182 501	216 598
Power, P (W)	145	140.4	18 072	17 165	31 520	30 943
Uncertainty (%)	±1.8		±2.6		±0.9	

constant above 10^{-7}. According to an Eulerian approach, results are then transformed back into the stationary frame. The stirring geometry has been built with Gambit® software for the three scales: **a**, **b** and **c**. Thanks to the periodic symmetry, only one-half of the vessel was modeled leading to a reduction of calculation time. The meshes used are tetrahedral and hexahedral. Additional mesh refinements near the walls of the vessel and near the stirrer were completed so that the accuracy in the high-velocity gradients zones was improved. The mesh at each scale has also been optimized in order to obtain accurate results in a shorter calculation time. The effect of grid size has been investigated in the case of laminar flow for a Newtonian fluid. The number of computational cells tested at each scale is summarized in Table 2. Composing the results for each scale, in terms of power consumption, shows that this variable varies very little with the grid size. Therefore, the solutions in this work are independent of grid size.

Freitas (1999) has checked the numerical uncertainty in the case of several existing codes: Fluent, Star-CD, N3S and CFD-ACE. The rules of numerical calculations recommended by Freitas (1999) have been followed in this study, which means that a second-order discretization scheme has been used. The solution is grid independent, iterative convergence has been accurately addressed, boundary conditions have been explained, and the existing code has been cited.

2.3. Experimental set-up for energy consumption measurements

Experiments were carried out in a thermostated stainless steel vessel, the dimensions of which are those of scale **a** (Fig. 1). The stirring system previously described is known as MIG propellers and the torque measurements have been performed with a torque-meter (F612 TC, 0–500 N) supplied by Robin Industries. The stirring motor (M2JA 100L4A) can deliver a maximum power of 2.2 kW at 1500 rpm. The fluid used for the experiments was a Newtonian one and its characteristics are summarized in Table 1. From the torque measurements, C, the power, P, can be calculated by subtracting to the torque measured in the empty vessel, C_0, as shown below

$$P = 2\pi N(C - C_0). \tag{7}$$

It is important to carry out these measurements with an industrial pilot in order to take into account the ball bearings and shaft perturbations that are present on an industrial scale. This has, nonetheless, some drawbacks as the non-transparent nature of the industrial vessel makes it impossible to carry out tracer tests or laser doppler measurements.

3. Results and discussion

3.1. The energy curve and the Metzner and Otto constant: simulations and experiments

As the simulations also involve non-Newtonian fluids, the following theoretical equations have been given for the case of a power-law fluid for the calculation of the Metzner and Otto constant at different scales.

The power consumption of the stirring system may be computed from the integration of the viscous dissipation function, Φ_v. For the general case of an incompressible and

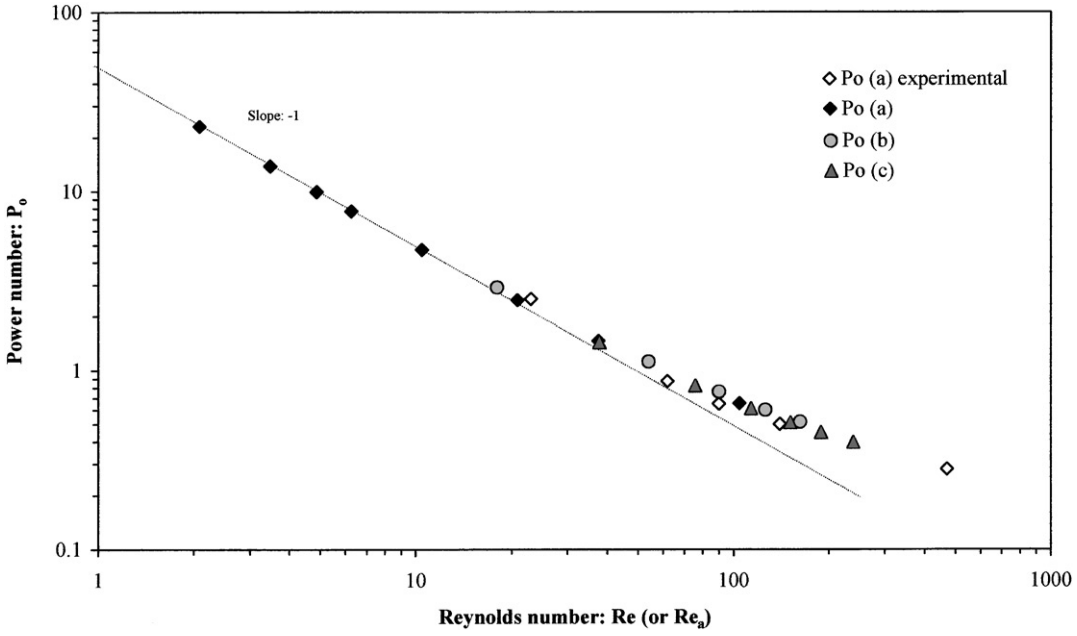

Fig. 2. Power curve, experimental results (scale **a**) and CFD results (scales **a**, **b** and **c**).

a power-law fluid (Ostwald–de Waele model), the power consumption can be expressed as

$$P = \int_{(V)} \mathrm{m}|\Phi_v|^{(\frac{n-1}{2})}\Phi_v \,\mathrm{d}V, \tag{8}$$

where

$$\Phi_v = \tfrac{1}{2}(\Delta : \Delta), \tag{9}$$

where Δ is the symmetrical rate of the deformation tensor.

The combination of Eqs. (8) and (1) enables the calculation of the dimensionless power number. In the case of Newtonian fluids ($n = 1$), this calculation has been repeated at each scale for several impeller speeds in order to plot the energy curve (i.e. P_o vs. Re). This curve, obtained from simulations with Newtonian fluids at scales **a**, **b** and **c** is compared in Fig. 2 to the one obtained from experiments conducted at scale **a** for Reynolds number varying between 20 and 500. Firstly, it is noticed that there is good agreement between experimental and simulated points although simulations involve a laminar model even in the transient regime. Secondly, the energy curves obtained at each scale have been superimposed which confirms, using a numerical approach in case of geometrical similarity, the energy curve is independent of the scales but is only a function of the stirring system geometry. The dimensionless analysis leads to an accurate evaluation of the power required, whatever the scale considered. Moreover, the points in laminar regime, $Re < 20$, are perfectly aligned as a straight line with a -1 slope, which is in full agreement with the theoretical Eq. (4). As expected, when the Reynolds number is increased, the regime becomes transient, and the points deviate from the slope -1.

Metzner and Otto (1957) characterized the fluid motion in the impeller region by an average shear rate, $\bar{\dot{\gamma}}$, which is linearly related to the rotational speed, N as shown below:

$$\bar{\dot{\gamma}} = kN. \tag{10}$$

The dimensionless average shear, k, commonly called the constant of Metzner and Otto, has been estimated for each scale. For this purpose, simulation of non-Newtonian fluids is required.

In order to calculate the Metzer and Otto constant, simulations have been conducted with different shear thinning fluids (Table 1), rheological behaviors of which can be described by the Ostwald–De Waele (or power law) models. For non-Newtonian fluids, the Reynolds number becomes the apparent Reynolds number, Re_a, which is a function of the apparent viscosity, μ_a. Substituting Eq. (10) into a simple power law leads to a generalized definition of the Reynolds number, Re_g as

$$Re_a = \frac{\rho N D^2}{\mu_a} = \frac{\rho N D^2}{m\bar{\dot{\gamma}}^{n-1}} = \frac{\rho N^{2-n} D^2}{m k^{n-1}} = Re_g k^{l-n}. \tag{11}$$

By introducing the power number, Eq. (11) can be rearranged as

$$P_o Re_g = P_o Re_a k^{n-1} = A k^{n-1}. \tag{12}$$

The energy curve of the DF stirring system, given by Fig. 2, can be extended to non-Newtonian fluids by the P_o vs. Re_a curve. For each scale, both the constants k and A have been calculated from simulations with shear thinning fluids by using Eq. (12). In case of experimental results, the constant A has been calculated using only the first two points since the last three points are in the transitional regime. All the results for A and k, compared in Table 3,

Table 3
Metzner and Otto constants, k, and laminar energy constants, A, for scales **a**, **b** and **c**

	Scales			
	a	**a**	**b**	**c**
Method used	Experimental	Simulations	Simulations	Simulations
Metzner and Otto constant, k	—	13	11	14
Laminar Energy constant, A	56	48	50	52
Correlation coefficient of $\ln(P_o Re_a)$ versus $n-1$	—	0.999	0.991	0.966

are very close. Nevertheless, the experimental value of A is slightly higher and this could be explained by the fact that the first two points are bordering on the laminar-transitional regime. Further experiments are needed in the laminar zone to obtain a better experimental accuracy.

In conclusion, it has been confirmed with a CFD approach that the energy curve as well as the dimensionless average shear in the vessel is specific to the stirring geometry only and not of the considered scale.

As the stirring system has been defined for industrial purpose and involves two kinds of impellers (DF and PBT), it is not surprising that no reference of this system is available in the literature. Among the rare references related to DF impellers, Käppel (1979) has studied the mixing of highly viscous Newtonian liquids. He presented a comparison between performances obtained by a helical ribbon and a stirring system involving five MIG DF impellers with D/T varying 0.9, 0.95 and 0.98. The constant A for a single stage can be estimated at 27 which is in agreement with the value given by the supplier. The value of A given by CFD (Table 3 and Fig. 2) for the stirring system (DF and PBT) is about 50 which would be close to the case of two stages of DF impellers. Höcker, Langer, and Werner (1981) have also studied stirring systems involving three DF impellers in baffled vessels. They compared the energy curves obtained in the case of Newtonian and, non-Newtonian liquids. They also proposed a value of the Metzner and Otto constant, k, equal to 11 which is quite close to those presented in Table 3.

Simulations of energy consumption allow the stirring speed to be set at every scale so that the power per unit volume can be kept constant during the scale-up. For this purpose, the power per unit volume has been plotted as a function of the stirring speed for the three scales in Fig. 3. In order to ensure a constant power per unit of volume for stirring conditions of 90 rpm at scale **a**, Fig. 3 shows that stirring speeds must be set at 70 rpm for scale **b** and 63 rpm for scale **c**. As expected, the variation of the power per unit volume as a function of the stirring speed presented in Fig. 3 differs because the Reynolds number involved at each scale is also different. For scale **a**, functioning at stirring speed smaller than 150 rpm, the regime is almost laminar ($Re < 10.4$) and the power per unit volume curve varies according to Eq. (5). For the other scales functioning at stirring speed larger than 20 rpm, the regime is rapidly transient ($Re > 40$) and the power exponent is enclosed between 2 and 3.

Consequences of a constant power per volume scale-up criteria, on the tip velocity, Reynolds, Froude and Weber numbers are summarized in Fig. 4. It has been noticed that there is a large increase in the Reynolds number, Froude number and tip velocity for the higher scales, **b** and **c**. As recommended by the suppliers and the common industrial users of DF impellers, the tip velocity can be set to 2–8 m s^{-1} and the stirring can be run both in laminar and transient regime. Because of these variations in Reynolds number, Froude number and tip velocity, the flow patterns in the vessel may also change during scale-up, leading to a change of mixing performances. In the following part, the effects of the constant per volume scale-up criteria combined with the geometrical similarity on the local analysis of the flow patterns will be assessed. It will be shown how the flow patterns change so that discussion on the pertinence of these scale-up rules is given. In addition, modifications of stirring systems are suggested for reducing the flow patterns changes during scale-up.

It is obvious that even the finest local flow pattern analysis will not be significant at an industrial process scale if this previous analysis has not been conducted. In the next part, it will be shown that flow pattern variations are significant from one scale to another despite the conservation of the power per volume unit.

3.2. Hydrodynamic results : flow pattern visualization of Newtonian fluids

The purpose of this section is to present the flow patterns of Newtonian fluids visualized in the vessels **a**, **b** and **c** in the case of a constant power per volume criteria (conditions of Fig. 4). Fig. 5 describes the planes of observation and the flow patterns at scales **a**, **b** and **c** are presented in Fig. 6. The colored scale refers to the dimensionless axial velocities, normalized by the tip velocity as ($v_z/\pi ND$).

The flow patterns differ between scales **a**, **b** and **c**. In the case of vessel **a**, particular oscillatory flows have been obtained. The fluid is put in motion only in front and behind the blades and no motion is noticed in plane 4. The areas of the axial cross section where the fluid flows up and down are linked to the position of the DF impeller. For the three scales, self-feeding at the tip of the DF impeller can be

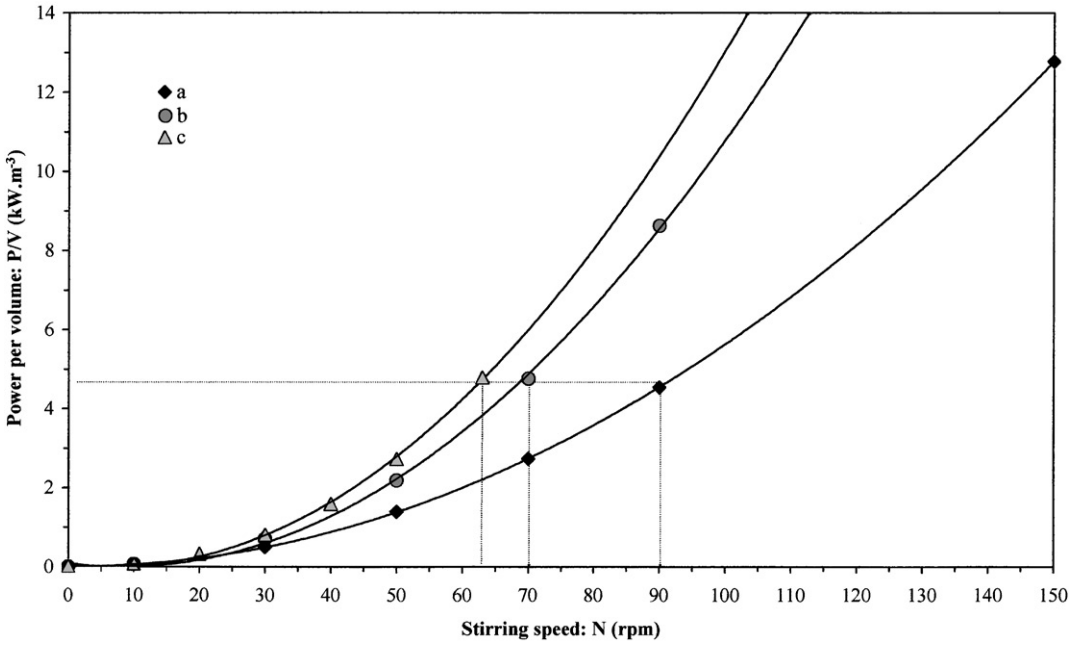

Fig. 3. Power per volume in function of stirring speed for scales **a**, **b** and **c**.

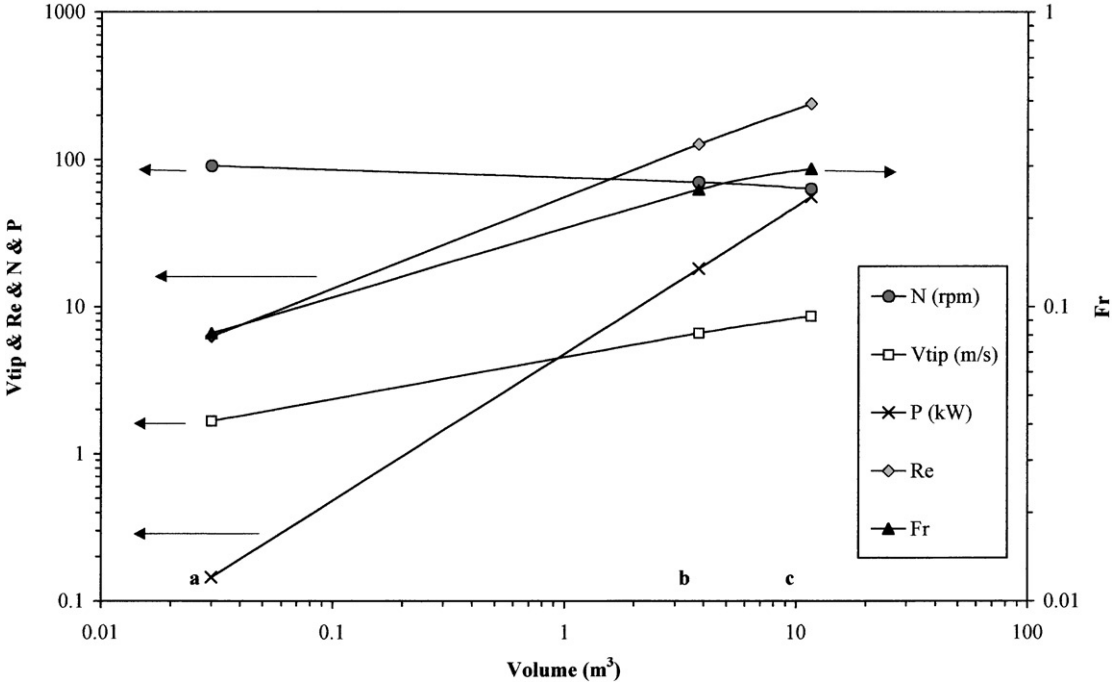

Fig. 4. Variations of several hydrodynamic parameters during scale-up.

observed. This is the main disadvantage of this kind of impeller. The mixing in the volume near the double-flux is not well renewed, particularly in laminar flow, even though the liquid is put in motion near the wall.

The axial velocity in each half-vessel has been averaged under the angular coordinate, θ with an in-house made program so that the normalized axial velocity ($v_z/\pi ND$) can be plotted for several horizontal planes. A comparison between scales, given in Fig. 7, shows that the axial flow at the smallest scale **a** (or lowest Reynolds number) is very poor in comparison with that obtained for scales **b** and **c**. The circulation loops are nonetheless well connected at each scale. Likewise, the flow generated by the down pumping PBT is more like that produced by a radial impeller. This is due to

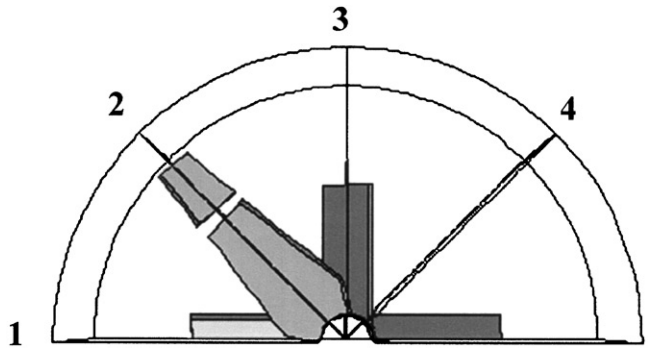

Fig. 5. Observation planes of flow patterns.

the proximity of the vessel base and the fact that the agitated fluid has a high viscosity. The unusual radial flow, provided by an axial impeller has already been noticed experimentally by Mavros, Xuereb, and Bertrand (1996) for an axial impeller in non-Newtonian liquids. In order to avoid such a phenomenon, one solution could be to move up this impeller stage in the vessel but this may induce a dead zone at the bottom of the vessel and, in this case, a third impeller has to be added. A secondary circulation loop, due also to radial flow, is observed in the plane above the DF impeller particularly when the Reynolds number is increased. This inaccurate hydrodynamic phenomenon could be avoided by increasing the impeller diameter.

Fig. 8 presents the contours of the dimensionless axial flow in the median plane located at equidistance between the DF and PBT impellers. The figure illustrates the phenomenon previously described in Fig. 6. The axial flow at small Reynolds number (scale **a**) is strongly dependent of the position of the impeller. At higher scales (**b** and **c**), this phenomenon tends to disappear because of the increase in the Reynolds number. Therefore, flow patterns then become more usual in all the vertical planes: the flow moves downward in the middle of the vessel whereas it moves upwards near the wall. The phenomenon characterizing scale **a** has also been reported by Lamberto, Alvarez, and Muzzio (1999) in an experimental and computational study of a stirring vessel in laminar flow. In the case of Rushton turbine, these authors have shown that the positions of segregated regions are found to move towards the impeller in the radial direction and away from the impeller in the axial direction as a blade approaches. They also noted that as the Reynolds number increases, this effect decreases; the structure becomes less dependent on the angular position of the blade.

In order to point out this phenomenon, the dimensionless axial flow in the median planes of each scale, for two different normalized radii ($\bar{r} = 0.4$ and 0.8, as indicated in the Fig. 8), are presented in Figs. 9 and 10, respectively. In the case of scale **a**, the dimensionless axial velocity at both radii $\bar{r} = 0.4$ and 0.8 varies around zero except in front and behind the DF impeller. It is then obvious that the averaging carried out to plot Fig. 7 leads to a reduction of the motion in the plane. The upward and downward flows near the DF impeller are namely added and, as the axial velocity in the rest of the angular co-ordinate range is close to zero, the resulting mean is very low. This is not the case for higher Reynolds numbers (i.e. scales **b** and **c**). Firstly, axial flow is of the same kind (positive or negative) before and after the DF impeller. Secondly, the dimensionless velocity is generally negative for $\bar{r} = 0.4$ and generally positive for $\bar{r} = 0.8$. In conclusion, the average along the angular co-ordinate θ, is only meaningful for higher Reynolds numbers, i.e. larger scales. Therefore, a new approach without angular averaging has been investigated and is detailed in Section 3.3.

The particular low flow pattern obtained at scale **a** is due to small Reynolds numbers and the same dimensionless flow pattern would be obtained for a higher scale if the Reynolds number was maintained constant, which is extremely exceptional in scale-up procedures. The flow pattern obtained at the smallest scale **a** is not representative of those obtained after scale-up. Therefore, a distortion of geometrical similarity or a change in stirring geometry could be investigated at the smaller scale in order to provide closer flow patterns between pilot and industrial scales. Generally, these kinds of distortions are very common in industrial cases and this is the reason why a numerical approach like the one developed in this paper is very useful.

3.3. Quantitative approach: calculation of the axial and tangential average flow numbers and the average swirl number

The flows provided by a stirrer are usually characterized by a pumping number approach, which considers the flows through a volume close to the agitator. This approach becomes unsuitable in the case of multi-staged and large diameter impellers and, particularly, in case of laminar flows presented here (with re-circulation loops). Therefore, a more global approach is needed. In order to evaluate the global efficiency of the whole considered stirring system at these three different scales, the upward or downward axial flows, Q_{ax}, have been computed for several heights, z, of the

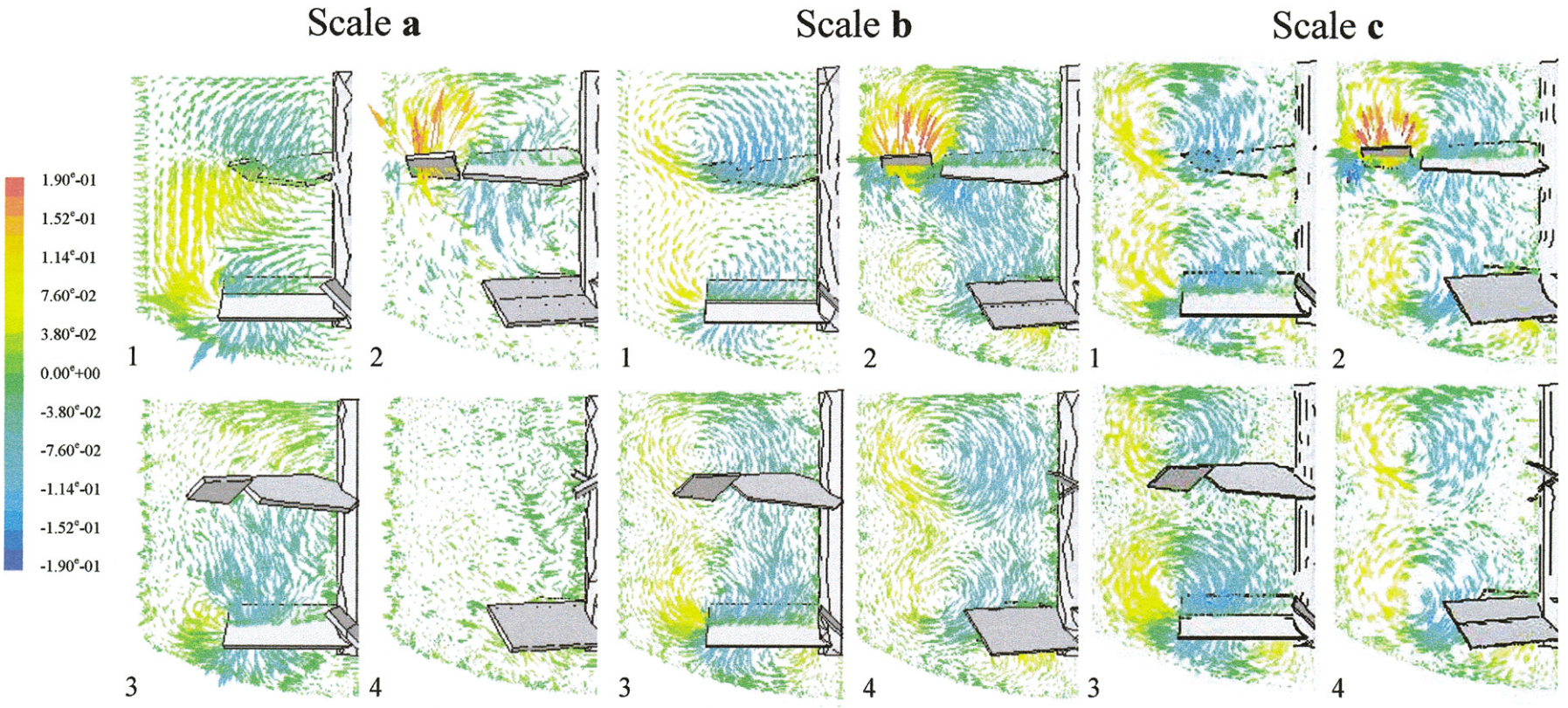

Fig. 6. Flow patterns (v_z/V_{tip}) in vertical planes of stirring vessels **a**, **b** and **c** for a constant power per volume scale-up criterion.

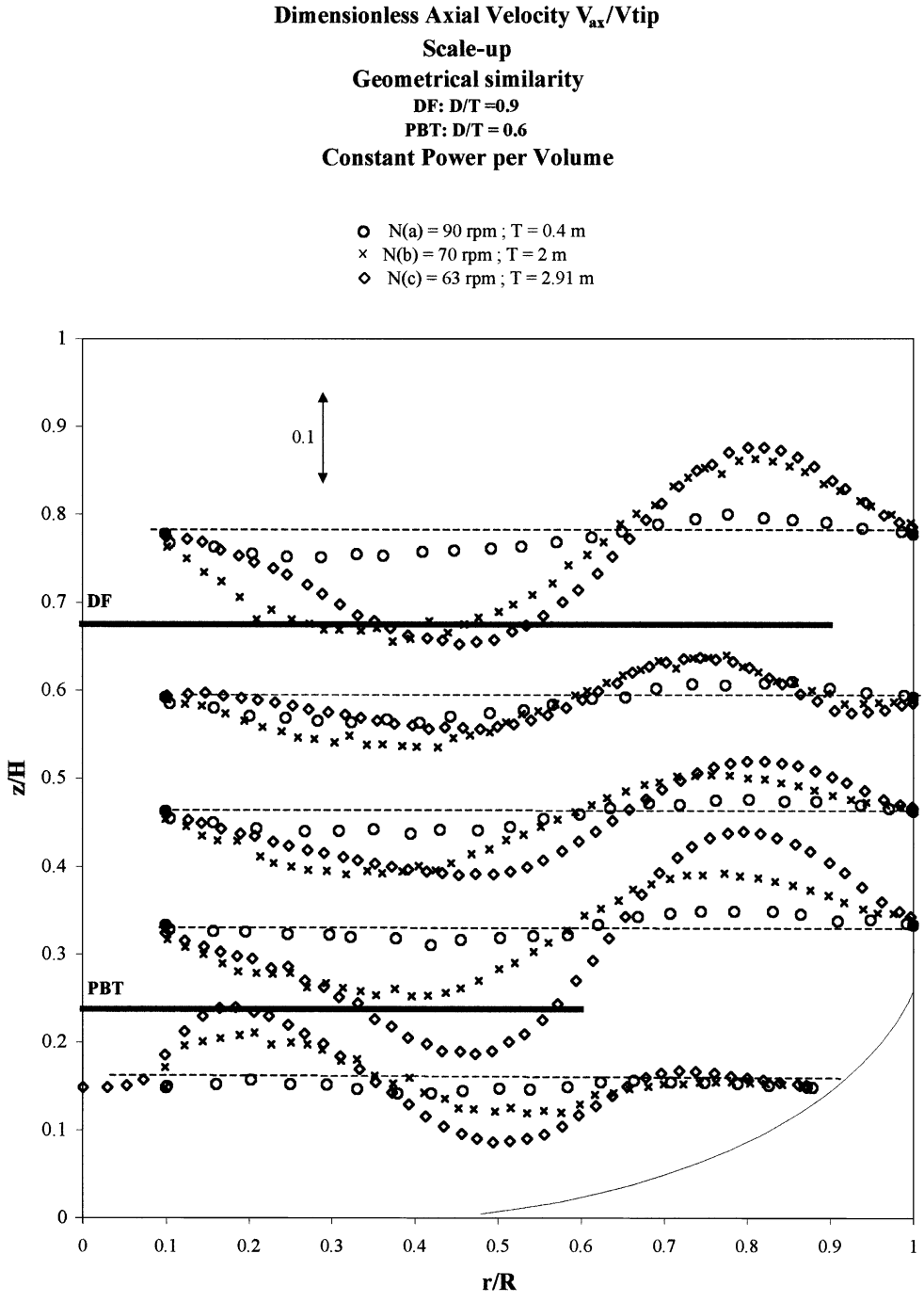

Fig. 7. Angular average of flow pattern at the scales **a**, **b** and **c**.

vessels. As it has been shown in the previous part, the angular average of the axial velocity is not suitable for the case of very small Reynolds number. Therefore, axial flows have been computed without taking into account the angular position of velocity vectors, but only their sign as given by

$$Q_{\mathrm{ax}} = \sum_{i/v_i>0} A_i v_{zi} = \sum_{i/v_i<0} A_i v_{zi} \tag{13}$$

where A_i is the computational cell area.

The dimensionless axial flows numbers, $N_{q\,\mathrm{ax}}$, given by Eq. (14) can then be plotted as a function of the dimensionless height z/H for several impeller speeds (or Reynolds number):

$$N_{q\,\mathrm{ax}} = \frac{Q_{\mathrm{ax}}}{ND^3}. \tag{14}$$

For a constant power per volume criterion (conditions given by Fig. 4), the axial flow numbers are plotted in Fig. 11 as a function of the dimensionless height, z/H. Like the

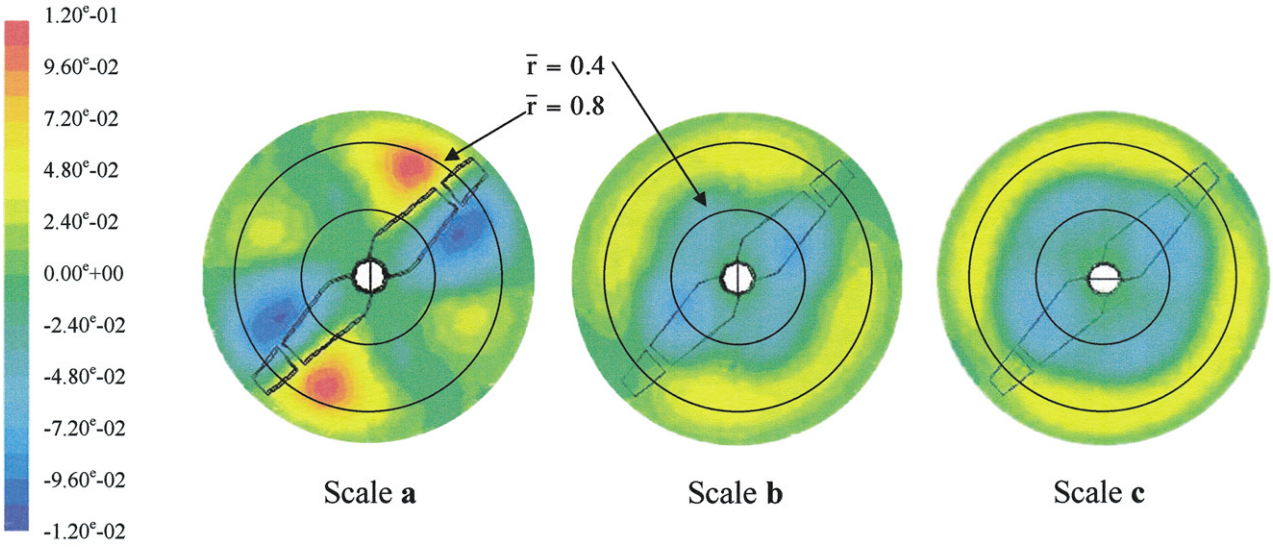

Fig. 8. Contours of dimensionless axial velocity (v_z/V_{tip}) visualized in the median planes between DF and PBT impellers (Iso-$z/H = 0.46$).

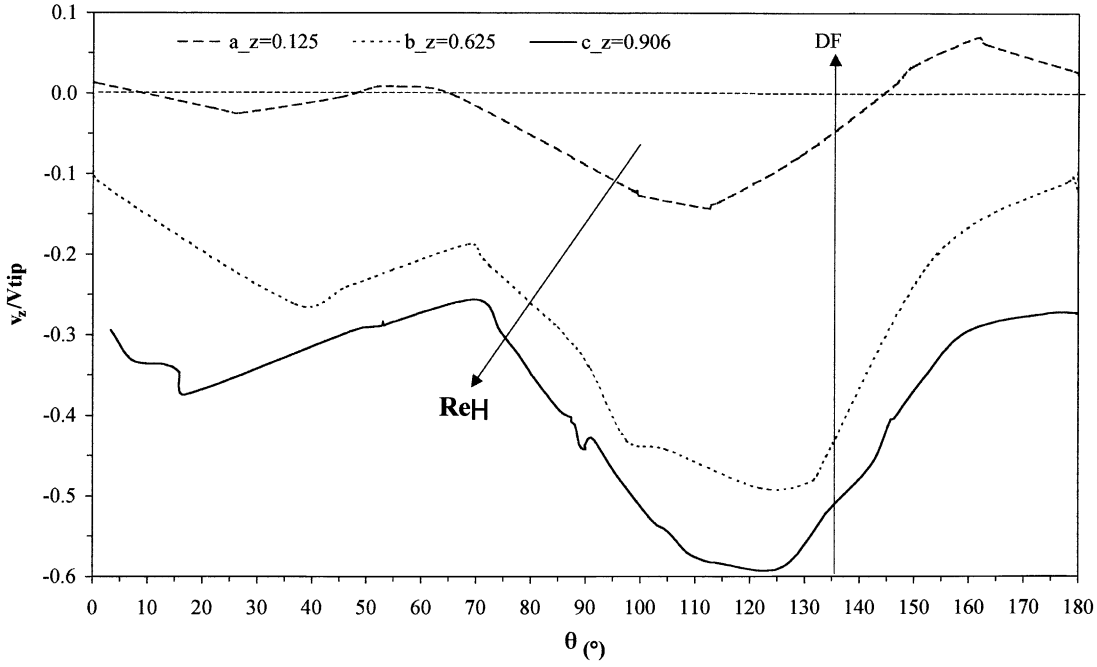

Fig. 9. Variation of the dimensionless axial velocity (v_z/V_{tip}) along angular co-ordinate for $\bar{r} = 0.4$ in the median planes between the DF and PBT stirrers.

flow patterns, the shapes of the curves differ from scale **a** to scale **b** and from scale **b** to scale **c**. This is obviously due to a change in the hydrodynamic regime. The pitched blade turbine (PBT) and the double-flux (DF) stirrers are positioned at $z/H = 0.24$ and $=0.69$, respectively. The axial flow at scale **a** is characterized by minima, which occur at heights corresponding to the stirrer planes. In these planes and at low Reynolds numbers, the stirrers generate tangential and radial motion. Therefore, it is recommended to modify the angles of the impeller blades in order to provide more conventional axial flow in laminar range. The curves related to **b** and **c** have almost the same shapes even though the regime becomes less and less laminar from **b** to **c**.

In order to check the continuity of the curves, $N_{q\,ax}$, between the scales, several agitator speeds have been simulated so that the curves $N_{q\,ax}$ vs. z/H can be compared for different Reynolds number values (Fig. 12). In the case of scale **a**, it has been observed that the dimensionless values and the shape of the curves are the same whatever the impeller speeds when the Reynolds number is smaller than 20. The shape of the curves related to the scale **b** are close to those of **a** or **c** depending on the Reynolds number.

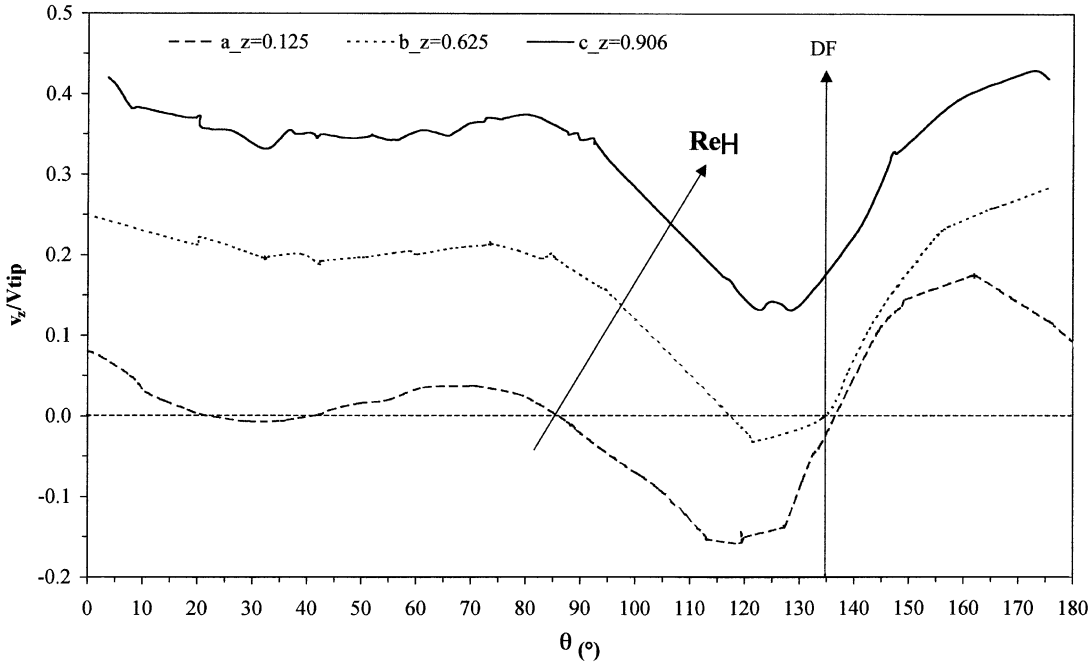

Fig. 10. Variation of the dimensionless axial velocity (v_z/V_{tip}) along angular co-ordinate for $\bar{r}=0.8$ in the median planes between the DF and PBT stirrers.

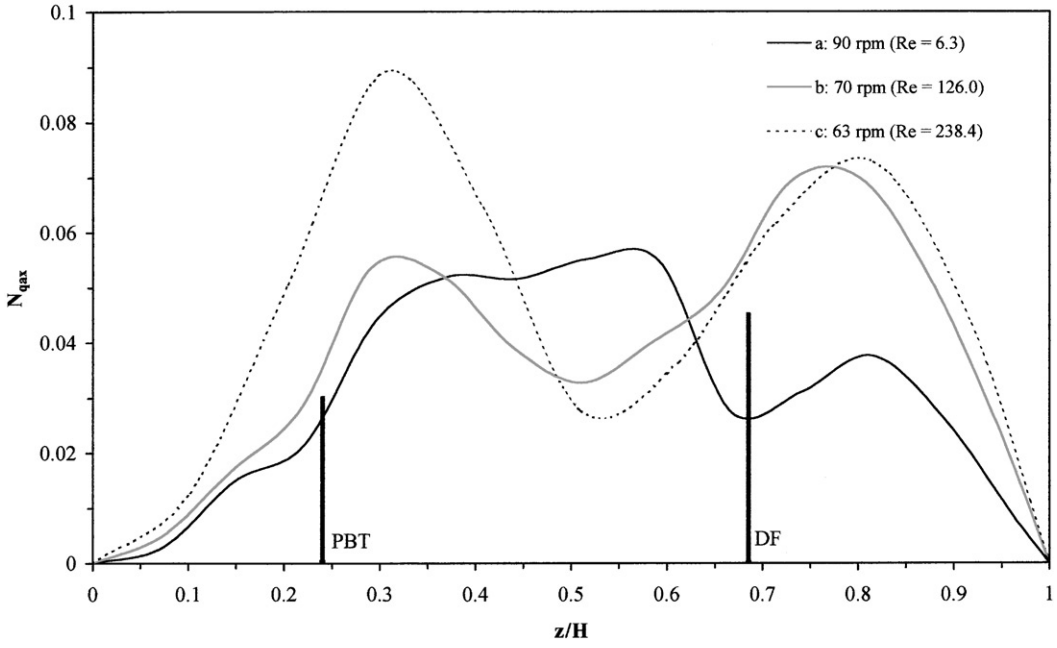

Fig. 11. Dimensionless axial flow profile in vessels **a**, **b** and **c** for a constant energy per volume.

The presence of these two kinds of curves is in agreement with this qualitative approach since the first type of curve is typical of the laminar flow ($Re < 20$) and corresponds to the oscillatory flow observed in the case of scale **a** (Fig. 3). The second kind of curve corresponds to the transient regime, which leads to more usual flow patterns. One could expect also to identify a characteristic curve for the turbulent regime. Further simulations would be needed to confirm it.

The dependence of the flow of the Reynolds number can also be shown by plotting global hydrodynamic criteria related to the height of the vessel as a function of the Reynolds number. The average axial flow number, $N_{Aq\,ax}$, has also been computed by averaging the curves Q_{ax} vs. z, and by

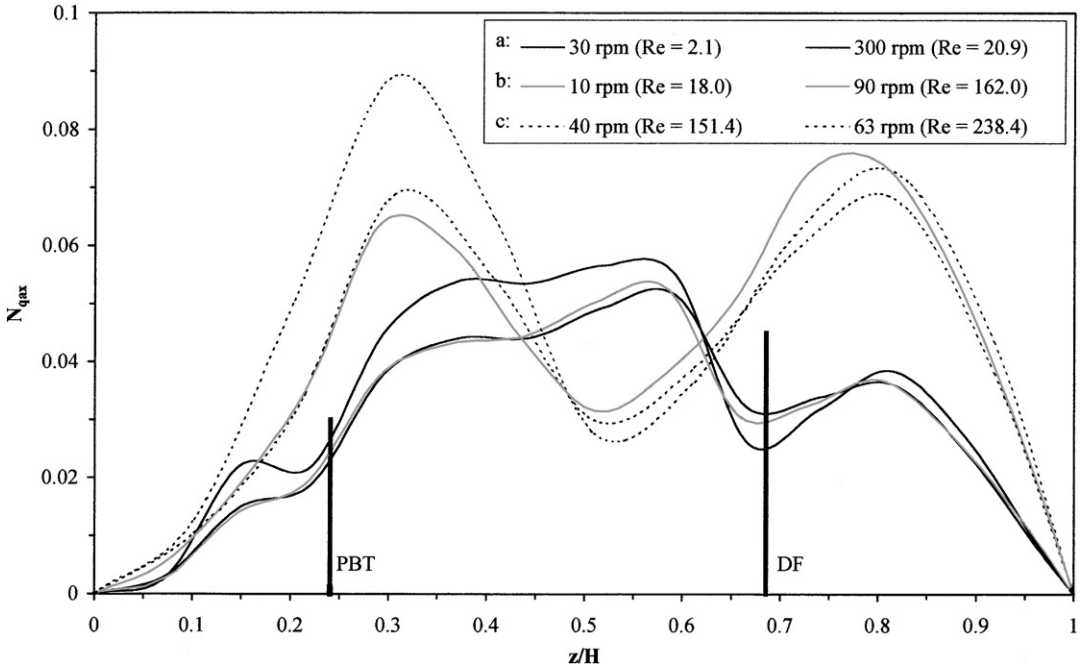

Fig. 12. Dimensionless axial flow profile in vessels **a**, **b** and **c** for several Reynolds numbers.

normalizing the result by ND^3 as shown in (15). The average tangential number, $N_{Aq\,\tan}$ has also been calculated for each case as in Eq. (16):

$$N_{Aq\,\mathrm{ax}} = \frac{1}{ND^3}\,\frac{\int_0^h Q_{\mathrm{ax}}(h)\,\mathrm{d}h}{\int_0^h \mathrm{d}h}, \tag{15}$$

$$N_{Aq\,\tan} = \frac{Q_{\tan}}{ND^3}. \tag{16}$$

By dividing the average axial number by the average tangential number, a new criterion is introduced, given by Eq. (17), which is derived from the Swirl number introduced by Bakker and Van Den Akker (1994):

$$S_A = \frac{N_{Aq\,\mathrm{ax}}}{N_{Aq\,\tan}}. \tag{17}$$

This dimensionless number, named Average Swirl number, illustrates the capability of the stirrer to convert tangential motion into axial motion. The main advantage of these three global dimensionless numbers is that the flows can be characterized in the entire vessel and not only in the volume surrounding the impeller.

These three global parameters are plotted in Fig. 13 as a function of the Reynolds number for scales **a**, **b** and **c**. Continuity between scales can be verified. The results are in agreement with the LDV measurements run by Mavros et al. (1996). They confirm that an increase in the Reynolds number improves axial flow. A minimum value of S_A at a Reynolds number equal to 30 can be noticed. This minimum corresponds to a change of regime. This is the point from which the flow becomes independent of the blade position. In the range of Reynolds number lower than 30, the Average Swirl number increases when Reynolds number is reduced. In this domain, the tangential motion increases faster than the axial motion when the Reynolds number increases. This can be explained by a raise of the segregated zone with stirring speed. The mechanical energy delivered by the stirrer makes the tangential motion of this segregated zone higher, which reduces mixing performances. From an energy point of view, it is better, in this laminar zone, to set a low stirring speed.

A more convenient way to present the result, from a global hydrodynamic point of view, could be achieved by introducing the average axial circulation time which can be calculated from Eq. (18).

$$t_{\mathrm{ax}} = \frac{N_{Aq\,\mathrm{ax}}}{V}. \tag{18}$$

The dimensionless homogenization number given by Eq. (19) can then be introduced.

$$N_R = N t_{\mathrm{ax}}. \tag{19}$$

This number is very useful as it represents the number of revolutions for the materials to recirculate by the stirring system. Fig. 14 shows the variation of the recirculation number as a function of the Reynolds number. As expected, continuity is verified and the variation is very similar to the variation of $N_p t_m$ where t_m is the mixing time (Novak & Rieger (1969) the case of a screw). The recirculation number is constant in the laminar regime and would decrease regularly to a value which remains constant when the turbulent regime is attained. In addition to increasing strongly the stirring speed at the scale **a**, the simplest way to ensure the same kind of flow pattern consists in a distortion of the geometrical similarity at the smallest scale. Further

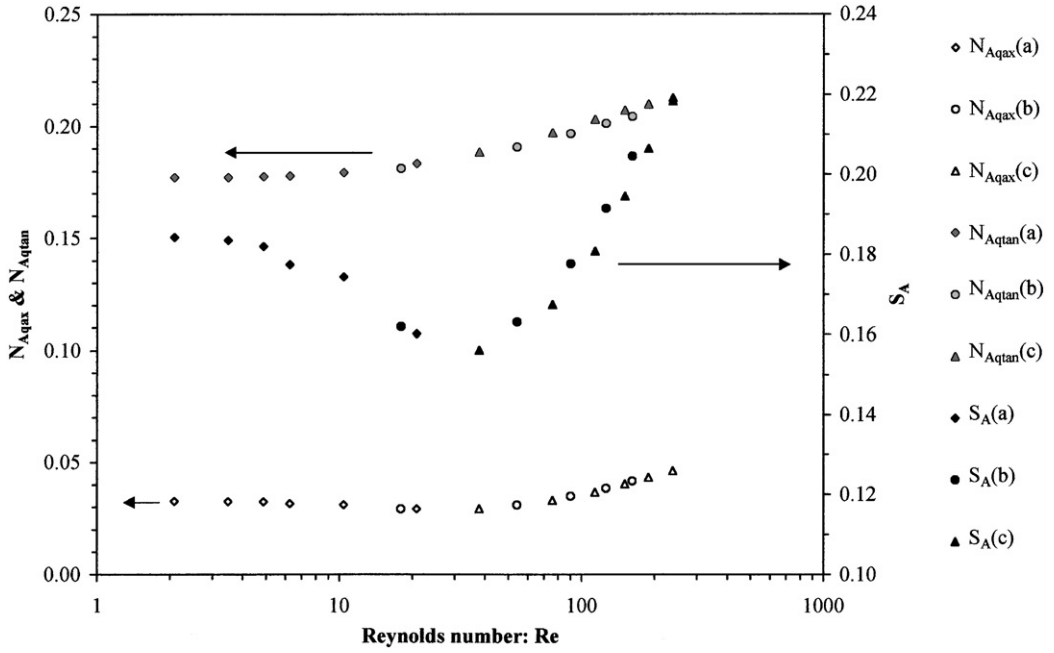

Fig. 13. Flow characterization, average axial and tangential numbers and Average Swirl number as a function of Reynolds number.

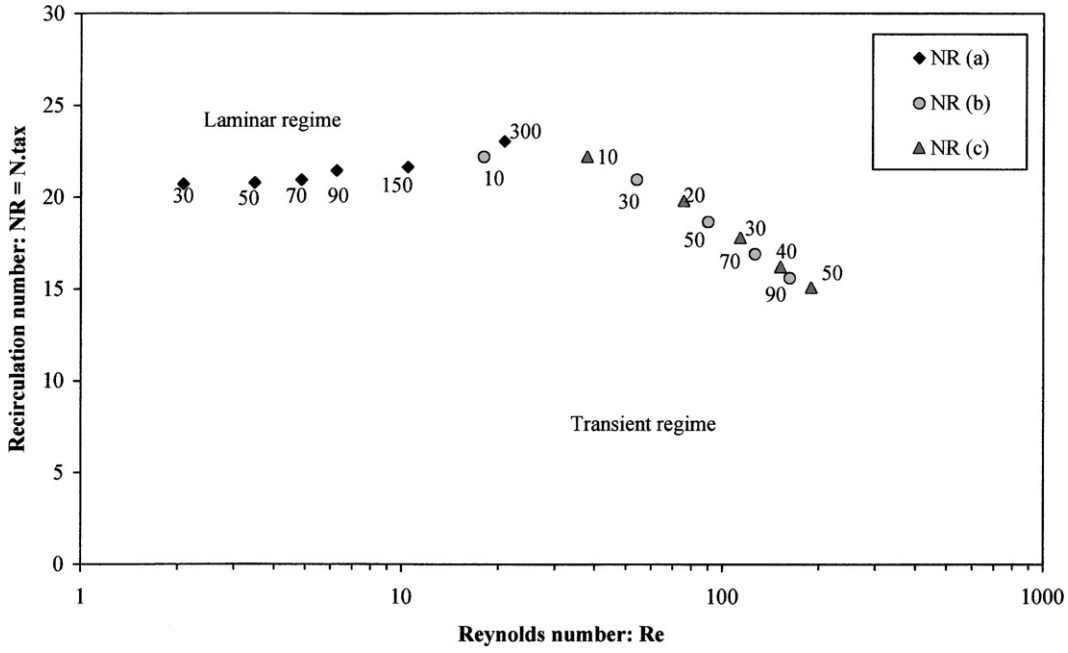

Fig. 14. Recirculation number as a function of Reynolds number.

simulations will be conducted with three bladed DF propellers equipped with deflector to limit radial flow. The width of the blades will be enlarged giving a high solidity ratio which limits oscillatory flow by forcing the axial downward motion. A deflector at the extremity of the downward blades will be added to limit the radial flow in laminar regime. Another interesting similarity distortion would be to investigate the addition of a second DF impeller at scale **a**. Such stirring system would have certainly greater power requirements but this study has shown that power per volume should not be chosen as scale-up criteria from pilot to industrial scale.

4. Conclusions and further work

An unusual methodology of scale-up of laminar mixing applied to an industrial stirring device has been

presented using CFD. Such an approach could be very useful in the case of scaling process where the hydrodynamics are critical.

The main advantage of such a stirring system (PBT and DF) is its versatility for different hydrodynamic regimes. Therefore, this kind of stirring system may be applied to different industrial processes involving viscosity variation of mixtures like, for example, those found in the food industry or cosmetics, pharmaceutical, petroleum and polymer specialty industries.

Numerical results show good agreement with energy consumption measurements at the smallest scale **a** and so are assumed validated. As expected, the flow patterns depend on Reynolds number and then on the considered scale for power per volume as a scale-up criterion. New global criteria for characterizing multi-staged stirred systems have been introduced. Their values show two main functioning types, which are in good agreement with the qualitative results of the flow patterns in the vessel.

The most commonly used scale-up guidelines such as the geometrical similarity and the power per volume have been discussed regarding hydrodynamic considerations. Using the power per volume as a scale-up criterion, this study has shown that the flow patterns differ strongly from one scale to another. Therefore, it is suggested that this criterion must not be used without a preliminary study of the consequences on the flow pattern.

Two possible solutions could then be foreseen. On the one hand, modifications of the stirring geometry and functioning could provide closer flow patterns between each scale and, on the other hand, another scale-up criterion could be more appropriate.

According to Uhl and Von Essen (1986), the use of the power per volume constant rule provides a more than adequate power investment, and this means an excessive input of mechanical energy. Therefore, it would be interesting to study other scale-up criteria like constant tip velocity or constant torque per volume in further works.

However, the hydrodynamic study of flow patterns has shown that such a multi-stage double-flux stirrer leads to acceptable flow patterns for highly viscous mixtures in the case of the transient Reynolds numbers. Hydrodynamic performances are increased at higher scale. A distortion of the geometrical similarity has been suggested by modifying the double-flux impeller at the scale **a** in order to reduce the oscillatory flow. In the near future, the flow patterns generated by this new stirring system could be investigated with CFD and would be compared to the flow patterns presented in this study for the scales **b** and **c**.

As it is reminded by Dickey (2000), nearly all viscous fluid exhibit non-Newtonian characteristics. The study presented here could also be extended to the case of mixing scale-up of shear thinning fluids. In addition, such work performed here can be extended to other stirring systems such as screws, off-centered systems, special devices and all systems acting in transient flows.

Notation

a, **b**, **c**	names of the scales studied
A	laminar energy constant, dimensionless
A_i	cells area, m^2
C	torque, N m
C_0	torque measured in the empty vessel, N m
D	double-flux impeller diameter, m
D'	pitched blade turbine diameter, m
H	liquid height, m
H_1	height from the bottom of the pitched blade turbine, m
H_2	height between the pitched blade turbine and the double-flux impeller, m
i	calculation indice, dimensionless
k	Metzner and Otto constant, dimensionless
m	consistency index, kg $s^{n-2} m^{-1}$
n	flow behavior index, dimensionless
N	impeller speed, s^{-1} or rpm
P	power consumption, W
Q_{ax}	axial flow, $m^3\ s^{-1}$
Q_{tan}	tangential flow, $m^3\ s^{-1}$
r	radial co-ordinate, m
t_{ax}	average circulation axial time, s
t_m	mixing time, s
T	vessel diameter, m
v_z	axial velocity, m s^{-1}
V	vessel volume, m^3
V_{tip}	tip velocity, m s^{-1}
z	axial co-ordinate, m

Greek letters

α	linear scale-up factor
β	vessel form coefficient, dimensionless
Δ	symmetrical rate of deformation tensor, s^{-1}
θ	tangential co-ordinate, rad or °
Φ_v	viscous dissipation function, s^{-2}
$\bar{\dot{\gamma}}$	average shear rate, s^{-1}
μ	Newtonian viscosity, Pa s
μ_a	Apparent viscosity, Pa s
ρ	specific gravity, kg m^{-3}
σ	surface tension, N m^{-1}

Dimensionless numbers

Re	Reynolds numbers $(=\rho ND^2/\mu)$
Re_a	apparent Reynolds number $(=\rho ND^2/\mu_a)$
Re_s	generalized Reynolds number $(=\rho N^{2-n}D^2/m)$
P_o	power number $(=P/\rho N^3 D^5)$
Fr	Froude number $(=DN^2/g)$
$\bar{r}$	dimensionless radial co-ordinates $(=r/T/2)$
S_A	average Swirl number $(=N_{Aq\,ax}/N_{Aq\,tan})$
$N_{Aq\,ax}$	average axial pumping number $(=(1/ND^3)\int_0^h Q_{ax}(h)\,dh/\int_0^h dh)$

$N_{Aq\,\tan}$	average tangential pumping number ($=Q_{\tan}/ND^3$)
$N_{q\,\mathrm{ax}}$	axial pumping number ($=Q_{ax}/ND^3$)
N_R	recirculation number ($=N\,t_{\mathrm{ax}}$)

Acknowledgements

Financial support was provided by Cray Valley (ATOFINA) and the A.N.R.T. (Association Nationale de la Recherche Technique). Many thanks are specially due to the Process Engineering Group of Cray Valley Research Center for its contribution and technical assistance in this work.

References

Aubin, J., Naude, I., Xuereb, C., & Bertrand, J. (2000). Blending of Newtonian and shear-thinning fluids in a tank stirred with a helical screw agitator. *Transactions of the Institution of Chemical Engineers*, *78*(Part A), 1105–1114.

Bakker, A., & Van Den Akker, H. E. A. (1994). Single phase flow in stirred reactor. *Transactions of the Institution of Chemical Engineers*, *72*(Part A), 583–594.

Brito-de la Fuenta, E., Choplin, L., & Tanguy, P. A. (1997). Mixing with helical ribbon impellers: Effect of highly shear thinning behaviour and impeller geometry. *Transactions of the Institution of Chemical Engineers*, *75*(Part A), 45–52.

Dickey, D. S. (2000). Facing the challenge of mixing problem fluids. *Chemical Engineering*, *2*, 68–75.

Freitas, C. J. (1999). The Issue of Numerical Uncertainty. *Second international conference on CFD in the minerals and process industries*, CSIRO, Melbourne, Australia, 6–8 December (pp. 29–34).

Gerstenberg, H., Sckuhr, P., & Steiner, R. (1983). Stirred tank reactors for polymerization. *German Chemical Engineering*, *6*, 129–141.

Höcker, H., Langer, R. G., & Werner, U. (1981). Power consumption of stirrers in non-Newtonian liquids. *German Chemical Engineering*, *4*, 113–123.

Käppel, M. (1979). Development and application of a method for measuring the mixture quality of miscible liquids III. Application of the new method for highly viscous Newtonian liquids. *International Chemical Engineering*, *19*(4), 571–589.

Lamberto, D. J., Alvarez, M. M., & Muzzio, F. J. (1999). Experimental and computational investigation of the laminar flow structure in a stirred tank. *Chemical Engineering Science*, *54*, 919–942.

Mavros, P., Xuereb, C., & Bertrand, J. (1996). Determination of 3-D flow fields in agitated vessels by laser-doppler velocimetry: Effect of impeller type and liquid viscosity on liquid flow patterns. *Transactions of the Institution of Chemical Engineers*, *74*(Part A), 658–668.

Metzner, A. B., & Otto, R. E. (1957). Agitation of non-Newtonian fluids. *A.I.Ch.E. Journal*, *3*(1), 3–11.

Naude, I. (1998). *Simulations Directes de Mobiles en Cuve Agitée*. Contribution à l'Optimisation du Choix d'un Agitateur. Ph.D. thesis, INPT, France.

Novak, V., & Rieger, F. (1969). Homogenization with helical screw agitators. *Transactions of the Institution of Chemical Engineers*, *47*, 335–340.

Takahashi, K., Arai, K., & Saito, S. (1980). Power correlation for anchor and helical ribbon impellers in highly viscous liquids. *Journal of Chemical Engineering of Japan*, *13*, 147–150.

Tanguy, P. A., Thibault, F., La Fuente, E. B-De, Espinoza-Solares, T., & Tecante, A. (1997). Mixing performance induced by coaxial flat blade-helical ribbon impellers rotating at different speeds. *Chemical Engineering Science*, *52*, 1733–1741.

Uhl, V.W., & Von Essen, J.A. (1986). *Scale-up of equipment for agitating liquids*, *Mixing Theory and Practice*, Vol. 3 (pp. 199–264). New York: Academic Press Inc.